


## Article

# Preparation of High-Precision Dimension Seamless Thick-Walled Pipe by New Cold Rolling Process

Ran Li <sup>1</sup>, Xuewei Zhang <sup>1,\*</sup>, Cheng Zhang <sup>1</sup>, Jiaming Wang <sup>2</sup> and Jinfeng Huang <sup>1,\*</sup>

<sup>1</sup> State Key Laboratory for Advanced Metals and Materials, University of Science and Technology Beijing, Beijing 100083, China

<sup>2</sup> Pangang Group Jiangyou Changcheng Special Steel Co., Ltd., Mianyang 621701, China

\* Correspondence: zhangxueweisun@163.com (X.Z.); huangjf@ustb.edu.cn (J.H.)

**Abstract:** In this study, the cold rolling test on the quenched-tempered hot working die steel pipe with an outer diameter/thickness ratio of no greater than 3 was performed. The evolutionary trend of microstructure was examined by a combination of the microscope, SEM, and EBSD tests. The effect of feed rate on the inner wall roughness of rolled pipe was analyzed by means of white light interference. According to the experimental results, the maximum normal pressure per unit area increases from 1046.7 MPa to 1113.2 MPa with the rise in feed rate from 1 mm/stroke to 6 mm/stroke. Meanwhile, the inner wall roughness of the pipe declines from 0.285  $\mu\text{m}$  to 0.146  $\mu\text{m}$  after rolling. When the feed rate reaches 2 mm/stroke, the maximum normal pressure per unit area is 1058.4 MPa, which causes a significant plastic deformation to the inner wall of the pipe, and the average roughness below 0.2  $\mu\text{m}$ . The microstructure of the pipe is dominated by tempered sorbite whether before or after rolling, and the grain size before rolling is 16.22  $\mu\text{m}$  on average. After cold rolling, the longitudinal structure is deformed along the direction of rolling, in which the average grain size is 24.31  $\mu\text{m}$ . With the increase in deformation work-hardening behavior in the rolling process, the tensile strength improves from 1134 MPa to 1178 MPa, the yield strength increases from 985 MPa to 1125 MPa, and the room temperature impact energy diminishes from 58 J to 52.5 J. After vacuum tempering at 600 °C, it is difficult to eliminate the deformed band microstructure along the rolling direction completely. However, the grain size is reduced after cold rolling, no coarsening occurs, and the impact toughness increases from 52.5 J to 60.5 J. With the recovery of the original microstructure, the mechanical properties are restored to the before rolling level.

**Keywords:** cold pilger rolling; mechanical properties; microstructure; seamless thick-walled pipe



**Citation:** Li, R.; Zhang, X.; Zhang, C.; Wang, J.; Huang, J. Preparation of High-Precision Dimension Seamless Thick-Walled Pipe by New Cold Rolling Process. *Metals* **2022**, *12*, 1761. <https://doi.org/10.3390/met12101761>

Academic Editor: Mohammad Jahazi

Received: 18 August 2022

Accepted: 13 October 2022

Published: 19 October 2022

**Publisher's Note:** MDPI stays neutral with regard to jurisdictional claims in published maps and institutional affiliations.



**Copyright:** © 2022 by the authors. Licensee MDPI, Basel, Switzerland. This article is an open access article distributed under the terms and conditions of the Creative Commons Attribution (CC BY) license (<https://creativecommons.org/licenses/by/4.0/>).

## 1. Introduction

At present, high-precision thick-walled small-hole seamless steel pipes have been widely used in the production of various pneumatic or hydraulic components, such as air cylinders and oil cylinders. For their inner and outer diameters (ID and OD), high precision and small surface roughness are required [1]. The processing of thick-walled seamless pipes has direct effects on the surface quality of the inner hole, thus affecting the service life, accuracy, and reliability [2]. The core process of its manufacturing includes the formation of the hole and the processing of the inner surface. However, the traditional processing technology involves about 30 procedures, such as deep hole drilling, deep hole reaming, electrolytic polishing, honing, and inner hole processing. There were many process quality control points, and the product processing accuracy needs to be improved urgently [2].

To improve the efficiency of production as well as the dimensional accuracy and surface quality of seamless pipes, periodic cold rolling mills are often used [3]. The traditional cold rolling process is as follows: steel making → round steel rolling → piercing → pickling → cold rolling → annealing → polishing of the inner and outer surfaces. The main advantage of cold rolling is reflected in the following points. Firstly, the metal in

the deformation zone of cold rolling is subjected to compressive stress, which facilitates plastic deformation. Moreover, the metal can be rolled with significant deformation. The rolling elongation coefficient ( $\mu$ ) can reach 4~7, the rate of diameter reduction can reach 75–85%, and the deviation in wall thickness of the pipe after cold rolling is reduced. Cold rolling leads to a dense structure of the pipe and fine grain size. Moreover, the mechanical and physical properties of the pipe are improved simultaneously, for example, AISI 321 austenitic stainless steel pipes were rolled with  $Q = 1.15(Q = \ln(t_1/t_0)/\ln(d_1/d_0))$ , where  $t_0$  and  $t_1$  are the wall thicknesses before and after pilgering, and  $d_0$  and  $d_1$  are the average diameters before and after pilgering), and tensile strength increased from 581 MPa to 1096 MPa, [4]. However, most of the existing cold-rolled seamless pipes are thin-walled pipes [5]. For those specially made hydraulic seamless pipes, they have high hardness and strength, small inner diameter, and large wall thickness. Furthermore, the ratio of outer diameter to wall thickness is no greater than 3, it is difficult to cold rolling, and the mechanical properties of thick-walled and small-hole seamless pipes can be significantly affected by hydrogen embrittlement and intergranular corrosion during the pickling of waste pipes. Therefore, it is necessary to phase out pickling for a new way of producing high-precision small-hole thick-walled seamless pipes through cold rolling.

Therefore, to improve the preparation efficiency and surface quality of small diameter thick-wall seamless pipe and improve the surface quality of the thick-walled pipe. The emphasis discussed later will be on the determination of the optimum feed rate for industrial rolling the thick-walled pipe by evaluating the influence of feed rate on inner surface roughness, microstructure, mechanical properties, and rolling formability. Normal pressure per unit area, feed rate and surface roughness, and the relationship between microstructure and mechanical properties were discussed. Finally, the advantages and disadvantages of traditional machining, traditional cold rolling, and new cold rolling methods were investigated.

## 2. Materials and Methods

### 2.1. Experimental Material

Table 1 is the chemical composition of the experimental materials. Before cold working, it is also necessary to remove the iron oxide scale from the surface. The existence of iron oxide scale will reduce the quality of the subsequent lubrication, which compromises the surface quality of the steel pipe.

**Table 1.** Chemical composition of experimental materials (wt/%).

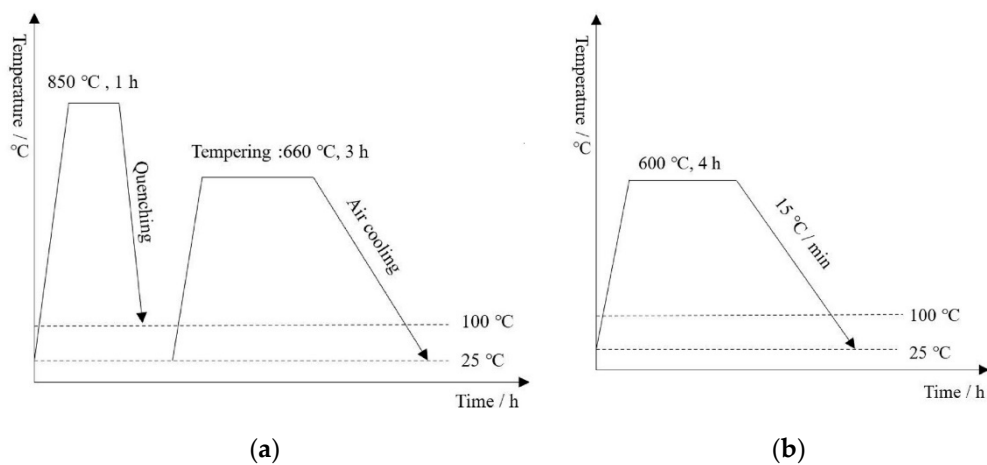
C	Si	Mn	P	S	Ni + Cr + Mo	W	V	Fe
0.29	0.19	0.14	≤0.015	≤0.015	5.0	0.37	0.63	Bal

### 2.2. Pilger Rolling and Heat Treatment

The production process of high-precision seamless steel pipe is as follows: quenching and tempering treatment → Mechanical honing → cold rolling → vacuum tempering → finished product. Table 2 is the list of parameters of cold rolling, the dimensions and inner wall roughness of mother pipe and finished pipe are all measured values, the feed rate is the set parameter, turn angle is from ref [6], working length of wall thickness reduction and roll die diameter are the measured values of the rolling tool. Figure 1 shows the heat treatment process diagrams of the experiment pipe before and after rolling. Vacuum tempering at 600 °C for 4 h, and then cooled down to room temperature by passing through room-temperature N<sub>2</sub> with a purity of no less than 99.99%, to avoid oxidation affecting the surface quality of the pipe.

**Table 2.** The parameters of the rolling experiment.

Mother pipe diameter	$\varnothing 46 \times \varnothing 18$ mm
Mother pipe inner roughness	0.7~0.8 $\mu\text{m}$
Mother pipe hardness	330~350 HV
Finished pipe after rolling	$\varnothing 33_0^{0.05} \times \varnothing 11_0^{0.05}$ mm
Feed rate: $m$	1~6 mm/stroke
Elongation of pipe: $\mu$	1.85
Stroke speed: $V_s$	80 strokes/min
Turn angle: $\theta$	$53^\circ$ [6]
Working length of wall thickness reduction	370 mm
Roll die diameter	300 mm

**Figure 1.** Heat treatment process diagrams of experiment pipe (a) quenching and tempering before rolling; (b) vacuum tempering.

### 2.3. Experimental Method

A tensile test was performed at room temperature on a CMT4103 computer-controlled electronic universal testing machine, with the strain rate set to 2 mm/min. Moreover, the impact test was carried out on a JBS-300B impact testing machine for a standard Charpy U-notch specimen. For the Charpy-U notch sample, most of the impact energy is consumed in the crack formation during the impact test, while for the Charpy-V notch sample, most of the impact energy is consumed in the crack propagation. For thick-walled pipes under high-pressure conditions, when cracks are formed, the pipes will be discarded, so Charpy-U notch samples are selected in this paper. The tensile and impact samples of each state are 3, and the average value is taken. After quenching and tempering, rolling and vacuum tempering, the samples were ground and polished, and corroded with 4% nitric acid alcohol solution, while their transverse and longitudinal microstructures were observed under optical microscope and ZEISS SUPR A55 scanning electron microscope. The roughness in the inner surface of the pipes was measured by using white light interferometry equipment (MicroXAM-3D) to describe the roughening quantitatively and qualitatively.

## 3. Results

### 3.1. Quality of Pipe after Rolling

Table 3 shows the evolutionary trend in size of the finished product after rolling. It can be found that the inner and outer diameters of the finished products meet the requirement of a smaller tolerance than 0.05 mm. When the feed rate ranges from 1 to 6 mm/stroke, the size of finished products after rolling by the same pair of rolls and mandrels shows no significant correlation with feed rate.

**Table 3.** The evolution of diameter with the increase in feed rate.

Feed Rate (mm/Stroke)	1	2	3	4	5	6
OD (mm)	33.02	33.03	33.04	33.01	33.02	33.03
ID (mm)	11.01	11.02	11.01	11.04	11.00	11.03

In this study, the surface roughness of the pipe was characterized by determining a number of statistical parameters as follows [7]:

(1) Maximum surface height parameter ( $R_z$ ). The  $R_z$  parameter refers to the sum of the absolute values of maximum surface peak height,  $R_p$ , and maximum surface valley depth,  $R_v$ , as defined in Equation (1).

$$R_z = R_p + |R_v| \quad (1)$$

(2) Mean surface height parameter ( $R_a$ ). The  $R_a$  parameter refers to the arithmetic mean of the absolute value of the height within an observation area as defined in Equation (2). It is used to describe how surface heights fluctuate around the mean plane.

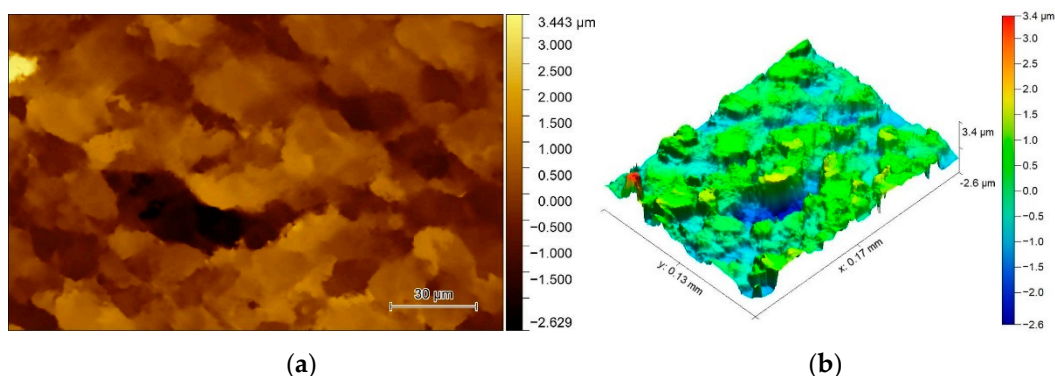
$$R_a = \frac{1}{n} \sum_{i=1}^n |\eta_i| \quad (2)$$

where  $n$  represents the total number of data points. The surface height  $\eta_i$  represents the height of each point from the mean plane, which is positive above the mean plane and negative below the mean plane.

(3) Root means the square value of surface heights ( $R_q$ ).  $R_q$  is equivalent to the square root of mean squares of the observed surface as defined in Equation (3).  $R_a$  and  $R_q$  are closely correlated with each other. It is a quadratic average of the asperities and may be applicable to identify the significant variations in surface characteristics.

$$R_q = \sqrt{\frac{1}{n} \sum_{i=1}^n |\eta_i|^2} \quad (3)$$

Figure 2 shows the topography at the inner surface of the mother pipe, with  $R_a$  0.789  $\mu\text{m}$ ,  $R_q$  0.769  $\mu\text{m}$ , and  $R_z$  1.59  $\mu\text{m}$ . Figure 3 shows the feed rate reaches 6 mm/stroke, the  $R_a$  0.146  $\mu\text{m}$ ,  $R_q$  0.182  $\mu\text{m}$ , and  $R_z$  0.46  $\mu\text{m}$ .

**Figure 2.** Cont.

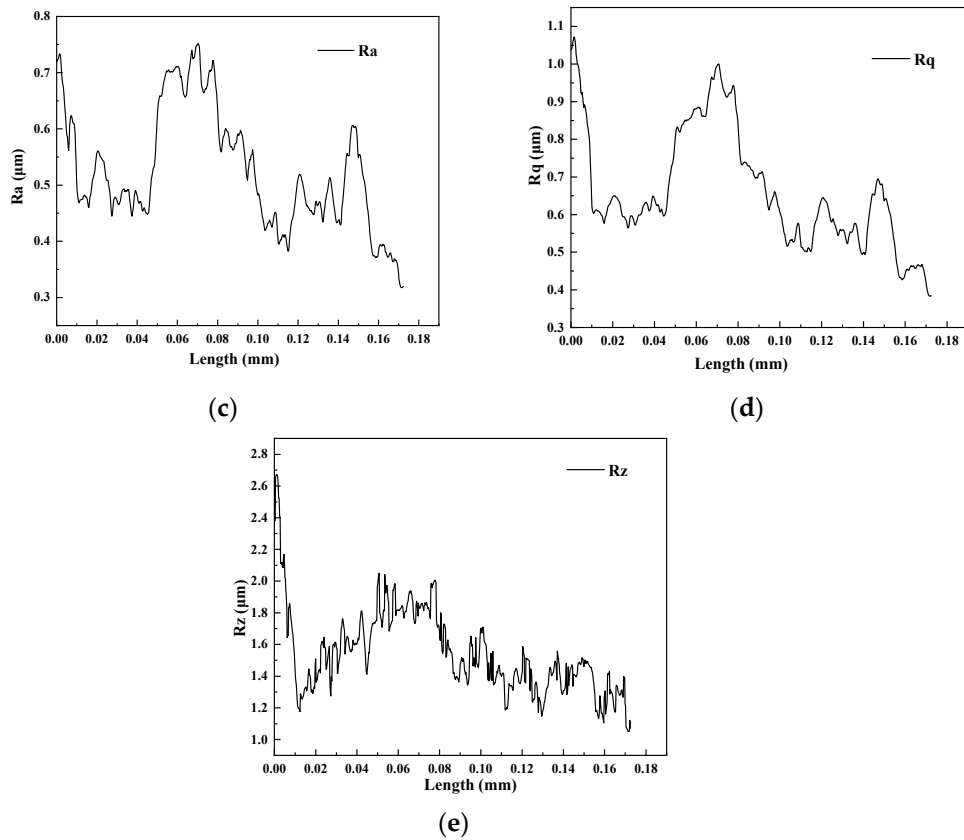


Figure 2. White light interference observation on the inner surface of after rolled pipe. (a) topography; (b) 3D morphology; (c)  $R_a$ ; (d)  $R_q$ ; (e)  $R_z$ .

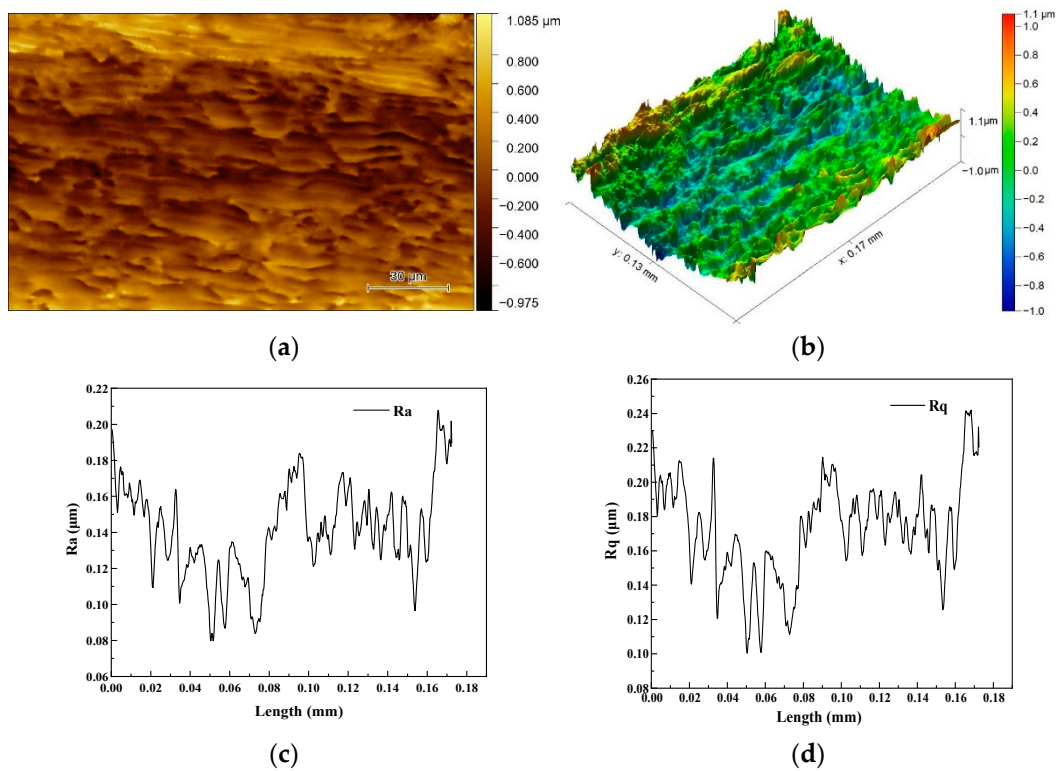
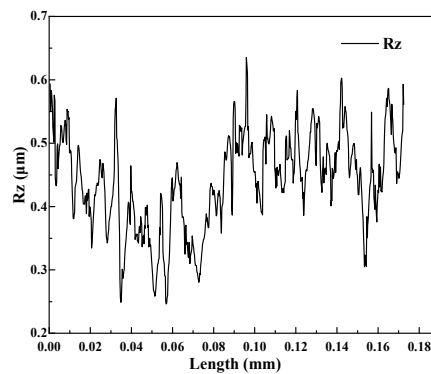


Figure 3. Cont.



(e)

**Figure 3.** White light interference observation on the inner surface of after rolled pipe. (a) topography; (b) 3D morphology; (c)  $Ra$ ; (d)  $Rq$ ; (e)  $Rz$ .

Surface roughness parameters ( $Ra$ ,  $Rq$  and  $Rz$ ) were extracted to quantify the change in roughening. On this basis, the relationship between the feed rate and surface roughness was established, as can be seen in Figure 4. With the increases in the feed rate, the roughness ( $Ra$ ,  $Rq$ , and  $Rz$ ) decreases gradually. When the feed rate ranges from 1 to 3 mm/stroke, the inner surface  $Ra$  of the pipe decreases from 0.285  $\mu\text{m}$  to 0.165  $\mu\text{m}$ ,  $Rz$  varies from 0.746  $\mu\text{m}$  to 0.485  $\mu\text{m}$ , and  $Rq$  varies from 0.318  $\mu\text{m}$  to 0.221  $\mu\text{m}$ , the roughness of the inner surface of the pipe decreases significantly. However, as the feed rate gradually increases to 6 mm/stroke,  $Ra$  of the pipe decreases from 0.165  $\mu\text{m}$  to 0.146  $\mu\text{m}$ ,  $Rz$  varies from 0.487  $\mu\text{m}$  to 0.485  $\mu\text{m}$ , and  $Rq$  varies from 0.221  $\mu\text{m}$  to 0.181  $\mu\text{m}$ , the reduction in the roughness tends to slow down. The reason may be that with the increase in the feed rate, the oil film thickness between the inner surface of the pipe and the mandrel increases. When the oil film thickness is too large, the reduction in the inner wall thickness will be affected [8–10], and the reduction trend of the roughness will slow down.

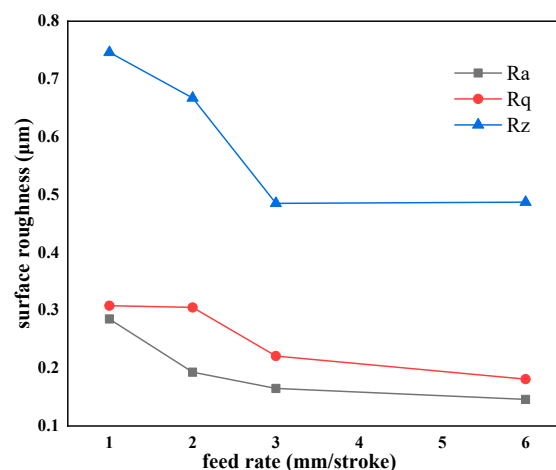


**Figure 4.** The evolution of surface roughness with the increase in feed rate.

The normal pressure per unit area ( $p_c$ ) under different feed rates in the rolling process is given by IOΦ Equations (4)~(8) [11]. The parameters and variables of the equation are presented in Tables 4 and 5. Figure 5 shows the curve of normal pressure per unit area plotted given different feed rates in the rolling process. It can be seen from the figure that the normal pressure per unit area increases rapidly in the case of forwarding rolling stroke, and that the normal pressure per unit area changes as the feed rate varies from 1 mm/stroke to 6 mm/stroke. The higher the feed rate, the greater the normal pressure per unit area. When the feed rate rises, the volume of metal compressed in a single pass increase,

thus resulting in a significant metal deformation and a sharp increase in normal pressure per unit area. The maximum normal pressure per unit area increases from 1046.7 MPa to 1113.2 MPa. When the maximum normal pressure per unit area reaches 1058.4 MPa (feed rate is 2 mm/stroke), the inner wall of the pipe suffers plastic deformation, and the roughness of the inner wall is lower than  $Ra$  0.2  $\mu\text{m}$ .

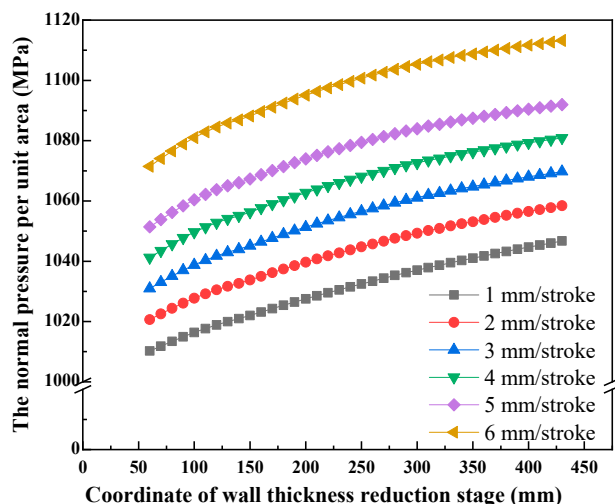


Figure 5. The curves of normal pressure per unit area in wall-reduction zone with different feed rate.

$$p_c = \sigma_b \cdot \left[ n_\sigma + f \left( \frac{s_0}{s_x} - 1 \right) \frac{\rho_x}{\rho_w} \cdot \frac{\sqrt{2\rho_x \Delta S_x}}{S_x} \right] \tag{4}$$

$$\Delta S_x = m\mu_x (tg\gamma_x - tg\alpha_x) \tag{5}$$

$$\mu_x = \frac{S_0(D_0 - t_0)}{S_x(D_x - S_x)} \tag{6}$$

$$tg\gamma_x = \frac{R_x - R_{x+1}}{L_x - L_{x+1}} \tag{7}$$

$$tg\alpha_x = \frac{r_x - r_{x+1}}{l_x - l_{x+1}} \tag{8}$$

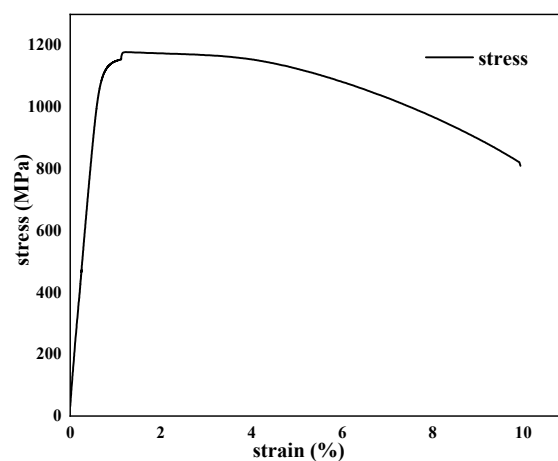
Table 4. Notation for Equations (4)~(8).

$p_c$	The normal pressure per unit area of the roll (mandrel) on the pipe	
$\sigma_b$	strength of the mother pipe under different deformations	Figure 6
$n_\sigma$	coefficient of principal stress	1.02~1.08 [11]
$f$	coefficient of friction between roller(mandrel) and pipe	0.1 [11]
$S_0$	the wall thickness of the mother pipe	14 mm
$S_x$	pipe wall thickness at position $x$	Table 5
$S_x$	the instantaneous reduction in wall thickness at position $x$	
$x$	roll groove radius at position $x$	Table 5
$w$	the radius of the drive gear pitch	140 mm
$\mu_x$	rolling elongation coefficient of pipe at $x$	
$\gamma_x$	taper between any $x$ and $x + 1$ positions at the ridge of the roll groove	Table 5
$\alpha_x$	taper between any $x$ and $x + 1$ positions at the ridge of the mandrel	Table 5
$R_x$	groove radius at any $x$ position of the roll groove	Table 5
$r_x$	radius at any $x$ position of the mandrel	Table 5
$D_0$	The outer diameter of the mother pipe	46 mm
$D_x$	pipe outer diameter at position $x$	Table 5
$L_x$	distance between any $x$ and $x + 1$ positions at the ridge of the roll groove	10 mm
$l_x$	distance between any $x$ and $x + 1$ positions at the mandrel	20 mm



**Table 5.** The value of variable.

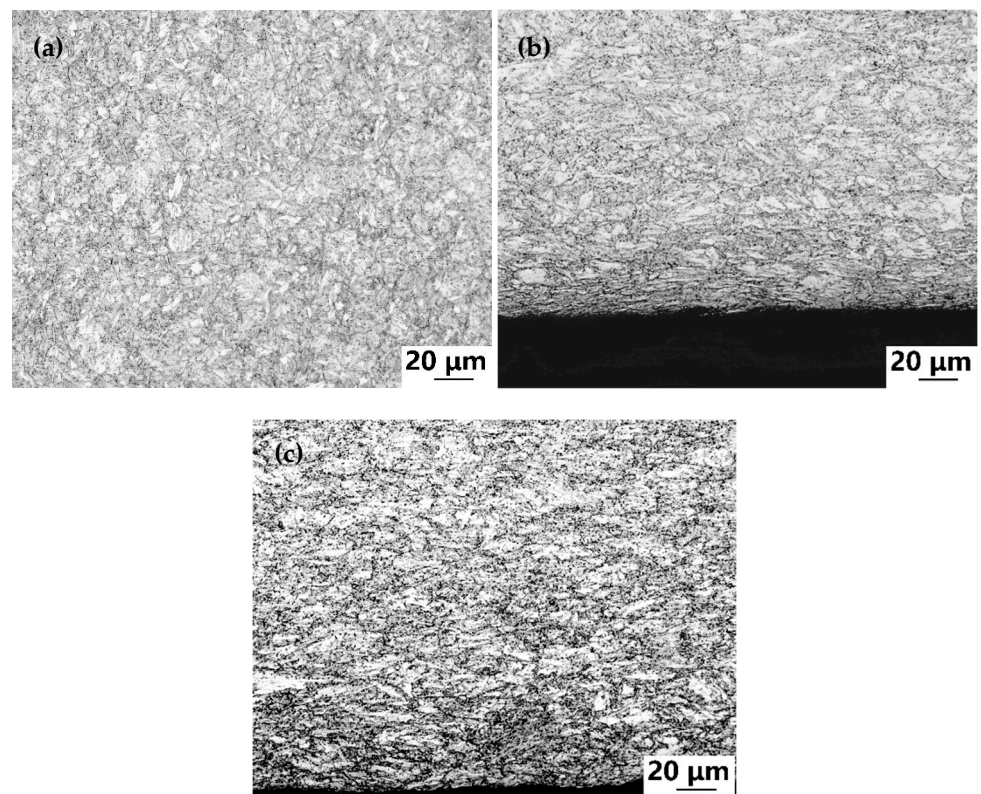
$D_x$ (mm)	$R_x$ (mm)	$\rho_x$ (mm)	$\gamma_x$ (mm)	$r_x$ (mm)	$\alpha_x$ (mm)	$S_x$ (mm)
42.514	20.257	129.743	0.0763	7.377	0.0082	13.88
41.805	19.902	130.098	0.0709	7.2975	0.00795	13.605
41.149	19.575	130.425	0.0656	7.22	0.00775	13.3545
40.546	19.273	130.727	0.0603	7.145	0.0075	13.128
39.997	18.998	131.002	0.0549	7.072	0.0073	12.9265
39.499	18.75	131.25	0.0498	7.001	0.0071	12.7485
39.054	18.527	131.473	0.0445	6.932	0.0069	12.595
38.66	18.33	131.67	0.0394	6.865	0.0067	12.465
38.316	18.158	131.842	0.0344	6.8	0.0065	12.358
37.996	17.998	132.002	0.032	6.7365	0.00635	12.2615
37.689	17.844	132.156	0.0307	6.675	0.00615	12.1695
37.395	17.698	132.302	0.0294	6.6155	0.00595	12.082
37.115	17.558	132.442	0.028	6.5575	0.0058	12
36.848	17.424	132.576	0.0267	6.5015	0.0056	11.9225
36.592	17.296	132.704	0.0256	6.4465	0.0055	11.8495
36.349	17.175	132.825	0.0243	6.3935	0.0053	11.781
36.118	17.059	132.941	0.0231	6.342	0.00515	11.717
35.898	16.949	133.051	0.022	6.292	0.005	11.657
35.689	16.845	133.155	0.0209	6.243	0.0049	11.6015
35.491	16.745	133.255	0.0198	6.1955	0.00475	11.55
35.303	16.651	133.349	0.0188	6.1495	0.0046	11.502
35.125	16.562	133.438	0.0178	6.1045	0.0045	11.458
34.957	16.478	133.522	0.0168	6.0605	0.0044	11.418
34.797	16.399	133.601	0.016	6.018	0.00425	11.3805
34.647	16.324	133.676	0.015	5.976	0.0042	11.3475
34.505	16.253	133.747	0.0142	5.9355	0.00405	11.317
34.372	16.186	133.814	0.0133	5.8955	0.004	11.2905
34.246	16.123	133.877	0.0126	5.8565	0.0039	11.2665
34.127	16.063	133.937	0.0119	5.8185	0.0038	11.245
34.015	16.008	133.992	0.0112	5.781	0.00375	11.2265
33.91	15.955	134.045	0.0105	5.7445	0.00365	11.2105
33.811	15.905	134.095	0.0099	5.7085	0.0036	11.197
33.717	15.859	134.141	0.0094	5.6725	0.0036	11.186
33.629	15.815	134.185	0.0088	5.6375	0.0035	11.177
33.546	15.773	134.227	0.0083	5.603	0.00345	11.17
33.467	15.734	134.266	0.0079	5.5685	0.00345	11.165
33.392	15.696	134.304	0.0075	5.534	0.00345	11.162
33.321	15.661	134.339	0.0071	5.5	0.0034	11.1605

**Figure 6.** Stress-strain curve of test steel.



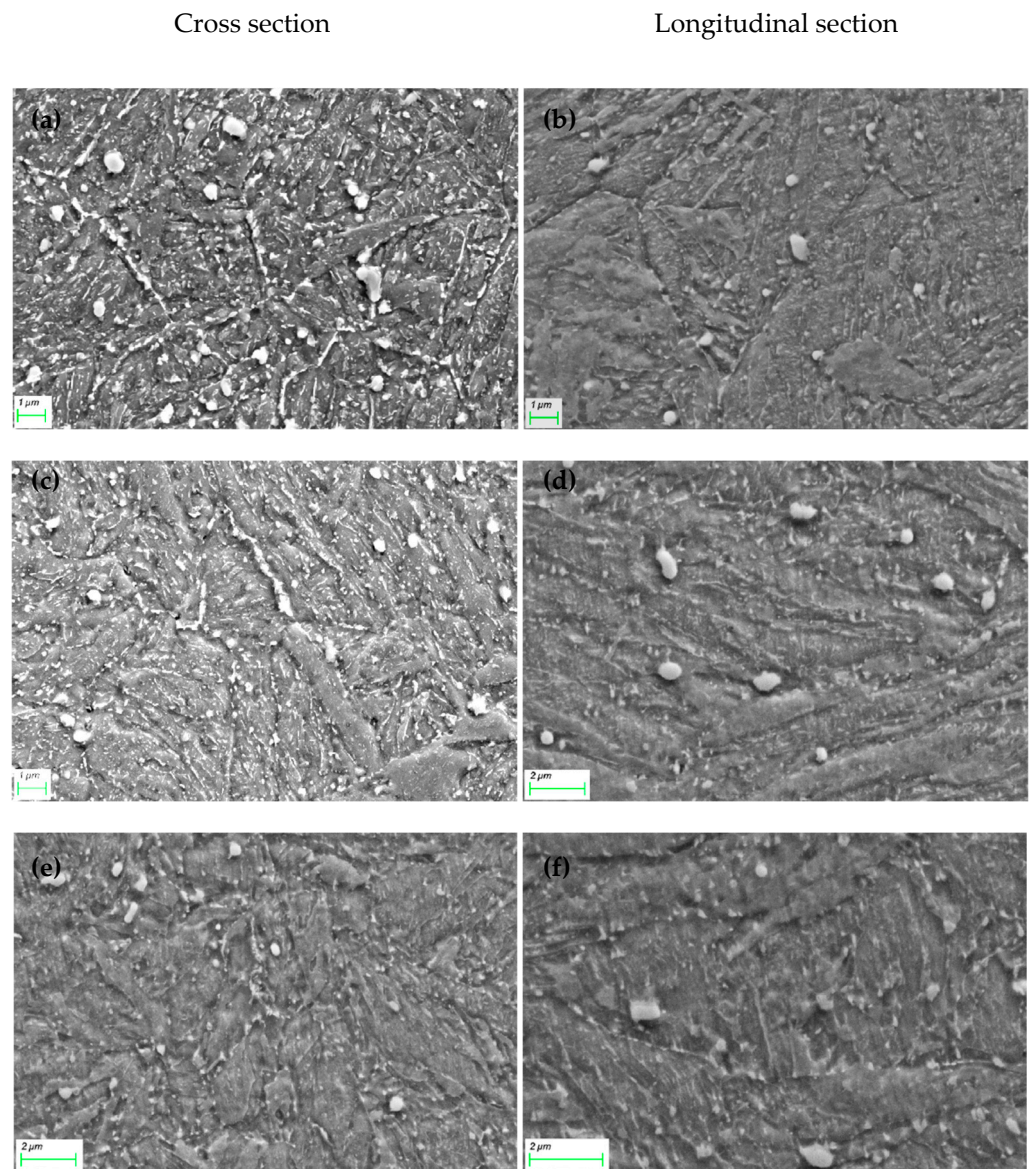
### 3.2. Microstructure Analysis

Figure 7 shows the microstructure as observed under the quenching and tempering state, after rolling states and vacuum tempering state, respectively. The room temperature microstructure of the quenching and tempering samples is dominated by tempered sorbite, and the grain size is  $16.22\ \mu\text{m}$  on average. The longitudinal microstructure of the cold rolling specimens showing deformation compared with the transverse microstructures, the equiaxed grains were deformed along the rolling direction, and the grain size before rolling is  $24.31\ \mu\text{m}$ . After vacuum tempering at  $600\ ^\circ\text{C}$ , the microstructure orientation relationship of the lath shape in the metallographic diagram of the tempered material still tends to the rolling direction. It can be observed that the obvious deformation bands cannot eliminate completely by vacuum tempering.



**Figure 7.** Microstructure of cross section near inner wall (a): quenching and tempering, (b): after rolling and (c): vacuum tempering.

Figure 8 shows the SEM morphology under the three processing states for the thick-walled pipe. The shape of carbides in the quenched and tempered state is characterized by long rods and needles, along with a small number of large-sized spheres and ellipsoids carbides. Moreover, there are some carbides distributed along the grain. Despite no obvious change in the shape of carbides in the rolling state after cold rolling, the carbides distributed along the grains were reduced, and the carbides in the longitudinal direction were distributed in a band shape along the direction of rolling. After tempering, the carbides were coarsened, no aggregation occurred along the grain, and the distribution of carbides was relatively uniform.



**Figure 8.** SEM morphology. (a,b) are quenching and tempering, (c,d) are after rolling, (e,f) are vacuum tempering.

Figure 9 shows the morphology and orientation distribution under the different extents of thickness reduction in pipe wall as characterized by using SEM and EBSD. As shown in Figure 9a, the grain morphology resembles a fine lath, and its orientation distribution is random before the rolling process in Figure 9c. As shown in Figure 9b,d, the grain orientation of after rolling is gradually focused on  $\langle 101 \rangle$ , and the distribution of grain orientation is highly consistent.



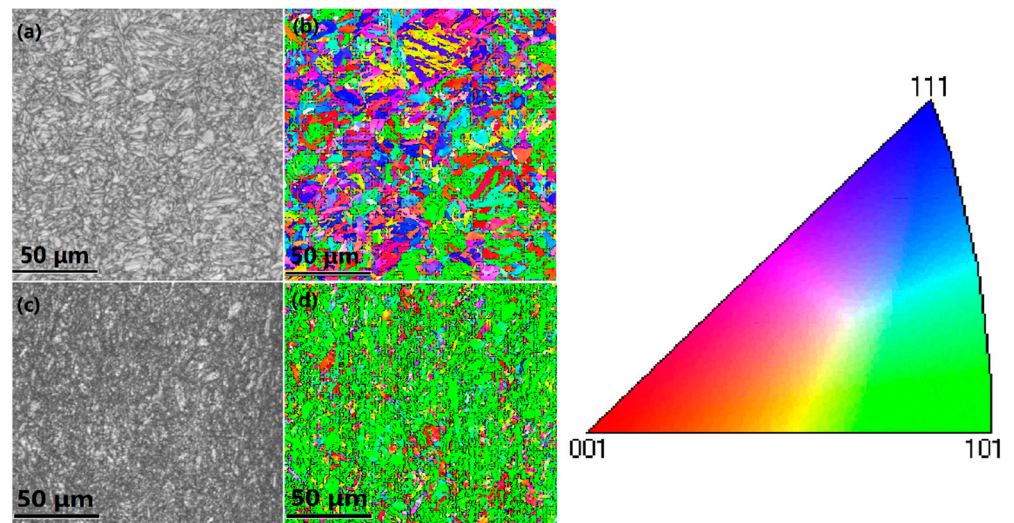


Figure 9. SEM and EBSD morphologies. (a,c) before rolling, (b,d) after rolling.

### 3.3. Mechanical Properties

Table 6 shows mechanical properties of materials before cold rolling. As deformation becomes more significant, the level of strength and hardness increases continuously in the process of cold deformation, but plasticity and toughness decline continuously. After rolling, the grain morphology is elongating along the rolling direction, a fibrous structure was formed due to significant cold deformation. Furthermore, the dislocation density also rose rapidly with the increasing severity of deformation, which is one of the main reasons for the occurrence of work hardening [12]. Due to the dislocation cells formed to hinder dislocation slip, the yield strength increases from 985 MPa to 1125 MPa, and tensile strength increases from 1134 MPa to 1178 MPa [13]. The yield strength decreases from 1125 MPa to 912 MPa, it is suspected that lots of dislocations occurring at grain boundaries in the cold rolling process recovery in the tempering process, and the dislocation density decreases.

Table 6. Mechanical properties of pipe in three conditions.

Conditions	$R_m$ (MPa)	$Rp_{0.2}$ (MPa)	$A$ (%)	$Z$ (%)	$A_{KU}$ (J)
Quenched and tempered	$1134^{+14}_{-18}$	$985^{+21}_{-16}$	$16_0^{+1}$	$59_0^{+3}$	$58^{+2.5}_{-0.5}$
Cold rolled	$1178^{+33}_9$	$1125^{+14}_{-18}$	$12.5^{+1.1}_{-0.4}$	$52_0^{+2}$	$52.5^{+1}_{-1.5}$
Vacuum tempered	$1055^{+23}_{-16}$	$912^{+26}_{-4}$	$20^{+1}_{-0.2}$	$65_0^{+1}$	$60.5^{+2}_0$

## 4. Discussion

### 4.1. Inner Surface Roughness of Pipe after Rolling

In the rolling process, when the feed rate increases gradually, the deformation rate of the metal rises at the same rolling speed. This is because of an increase in the volume of deformed metal between the roller and the mandrel. When the volume of deformed metal was too small, such as a feed rate 1 mm/stroke, the normal pressure per unit area in wall-reduction zone is 1046.7 MPa, the wrinkles generated by the compression of the inner wall cannot be flattened by the mandrel, resulting in an inner  $Ra \geq 0.2 \mu\text{m}$ . As the normal pressure per unit area increases, plastic deformation occurs in the inner surface of the pipe, and the height of the inner fold is reduced. When normal pressure per unit area in wall-reduction reached 1058.4 MPa, the roughness of inner wall was lower than  $Ra 0.2 \mu\text{m}$ .

### 4.2. Microstructure and Mechanical Properties

The microstructure of the parent tube is tempered sorbite with a grain size of  $16.22 \mu\text{m}$ . After cold rolling, the grain size is elongated to  $24.31 \mu\text{m}$  along the axial direction. Dur-

ing the cold rolling process, the tube deformation is strengthened, and  $Rp_{0.2}$  is increased from 985 MPa to 1125 MPa. As the dislocation movement resistance increases with the wall-reduction increasing, the resistance comes from the long-range resistance of elastic interaction between dislocations or the short-range resistance of the cut step during dislocation intersection.

Cold rolling is effectively an extrusion process that involves axisymmetric deformation. Such a deformation is the combination of one-way stretching and two-way compression. However, residual stress can arise due to cold rolling after plastic deformation. To address this problem, it is necessary to carry out vacuum tempering. The vacuum or high-purity N<sub>2</sub> gas tempering can be performed to maintain a low roughness in the inner wall of the seamless pipe. In practice, grain size change is an important index used to measure the degree of deformation. The grain size of the cross section and in the longitudinal direction was found closer and more uniform after cold rolling.

After vacuum tempering, the strength is slightly lower than the quenched and tempered material, but it is higher than the requirements on mechanical performance for the finished pipe with a tensile strength of 1030 MPa and a yield strength of 900 MPa. The impact toughness increases in tempered state, reaching 60.5 J. The tensile elongation (A%) and the percentage reduction in area (Z%) are higher than 10% and 40% in three states, which meets the practical requirements. The hardness at 600 °C for 4 h is 330~350 HV.

#### 4.3. Comparison of Three Preparation Process

Three preparation process flow charts are shown in Figure 10. In traditional machining process, the cutting chips will scratch the machined surface, thus increasing the roughness of the inner wall. Ultimately, the improvement of fatigue performance is hindered for the finished product. Moreover, due to the long pipe, the length of the matching tool holder will increase, which may lead to vibration and distortion during the processing. Consequently, the centerline of the inner hole will be skewed. However, it is difficult to ensure the deviation of the hole axis, which makes it necessary to take corrective measures to ensure its machining accuracy [14]. In order to ensure the high dimensional accuracy and surface quality of the inner hole, multiple passes of reaming and polishing are required in the follow-up. However, this incurs a lot of labor and time costs to process the slender pipe. There were about 30 procedures conducted from the start of deep-hole drilling on the round steel to final production. For example, during carbon steel deep-hole processing, the drilling rate was only 10~14 mm/min, but the deep hole drilling took 28~40 min [15] (pipe length is 400 mm). However, the inner hole roughness reached merely Ra0.4~0.8 μm after multiple reaming and polishing. Only electropolishing was possible given an inner surface roughness of no greater than Ra 0.2 μm [16].

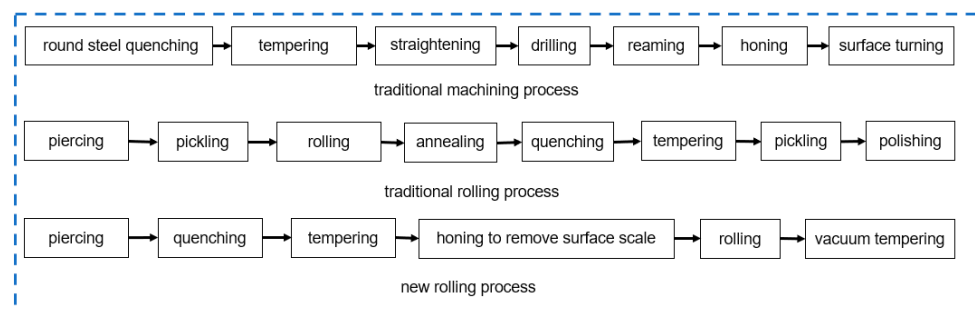


**Figure 10.** Flow chart of three preparation processes.

In the traditional rolling process, the pipe could be affected by hydrogen embrittlement and intergranular corrosion during the pickling, and most of the existing cold-rolled seamless pipes are thin-walled pipes. The traditional cold rolling process cannot produce

pipes with diameter thickness ratio  $\leq 3$  after tempering. Moreover, it also needs repeated heat treatment and polishing, so its preparation efficiency is lower than new rolling process.

The thick-walled pipe is prepared by new cold rolling, the average roughness of the inner wall of the finished product can be reduced to less than  $Ra0.2 \mu\text{m}$ . Calculate the rolling process time by Equation (9) with the feed rate increasing from 2 mm/stroke to 6 mm/stroke, the processing time decreased from 1.35 to 0.45 min, which is much better than traditional drilling in terms of preparation efficiency and the surface quality of finished product.

$$t = \frac{400}{\mu \cdot m \cdot V_s} \quad (9)$$

## 5. Conclusions

The effect of feed rate on the dimensional accuracy and inner wall roughness of cold rolled pipe was studied, and the effect of rolling on the microstructure and properties of the pipe was analyzed. The inner wall roughness of the mother pipe and rolled pipe was measured by white light interferometry. The characteristics of the pipes before and after rolling and after tempering, such as microstructure, tensile properties, impact toughness, etc., were investigated by SEM and EBSD.

- (1) Pilger cold rolling was performed to produce high-precision thick-walled and small-hole seamless steel pipes with a smaller diameter/thickness than 3, the inner and outer diameter tolerance less than 0.05 mm;
- (2) The relationship between the feed rate, normal pressure per unit area and inner wall roughness was analyzed. The results show that the feed rate is positively correlated with the normal pressure per unit area, and the increase in normal pressure per unit area is beneficial to reduce the inner wall roughness. When the normal pressure per unit area is up to 1058.4 MPa, inner wall roughness  $Ra \leq 0.2 \mu\text{m}$ ;
- (3) The microstructure of the mother pipe before rolling is tempered sorbite, and grain orientation is random distribution. After pilger rolling, the grain orientation is gradually focused on  $\langle 101 \rangle$ , and the density of dislocations increased continuously, resulting in work hardening behavior and decrease in plasticity and toughness, after vacuum tempering the dislocation density decreases, the strength decreases, and the plasticity and toughness return to the level before rolling;
- (4) The preparation efficiency and the surface quality of the thick-walled pipe by new cold rolling is much better than the traditional machining process and traditional rolling process.

**Author Contributions:** Conceptualization, J.H.; methodology, X.Z.; formal analysis, R.L.; investigation, R.L.; data curation, R.L.; writing—original draft preparation, R.L.; writing—review and editing, R.L. and X.Z.; visualization, R.L.; supervision, C.Z. and J.W.; project administration, J.H.; funding acquisition, J.H. All authors have read and agreed to the published version of the manuscript.

**Funding:** This research received no external funding.

**Institutional Review Board Statement:** Not applicable.

**Informed Consent Statement:** Not applicable.

**Data Availability Statement:** Not applicable.

**Conflicts of Interest:** The authors declare no conflict of interest.

## References

1. Akasaki, H. Progress in pipe and pipe technology and its future prospect—application and manufacturing. *Nippon Steel Tech. Rep.* **2004**, *90*, 75–81.
2. Huml, P.; Fogelholm, R.; Salwén, A. Optimization of cold rolling of precision pipes. *CIRP Ann.* **1993**, *42*, 283–286. [[CrossRef](#)]
3. Abe, H.; Furugen, M. Method of evaluating workability in cold pilgering. *J. Mater. Process. Technol.* **2012**, *212*, 1687–1693. [[CrossRef](#)]

4. Musazadeh, M.H.; Vafaei, R.; Mohammad Sharifi, E.; Farmanesh, K. Mechanical Properties, Microstructural Evolution, and the Effect of Friction on the Plastic Flow of the AISI 321 Austenitic Stainless Steel Tube During Cold Pilgering, An Experimental and Simulation Analysis. *Metall. Mater. Trans. B* **2018**, *49*, 3030–3042. [[CrossRef](#)]
5. Huang, B.; Huang, Q.; Li, C.; Liu, S.; Wu, Q. Effects of pipe rolling and heat treatment on microstructure and mechanical properties of CLAM rectangular pipe. *Fusion Eng. Des.* **2011**, *86*, 2602–2606. [[CrossRef](#)]
6. Gulyaev, Y.G.; Shifrin, E. Method of calculating the speed regime for continuous pipe rolling. *Metallurgist* **2014**, *57*, 904–910. [[CrossRef](#)]
7. Carneiro, K.; Jensen, C.P.; Jørgensen, J.F.; Garnces, J.; McKeown, P.A. Roughness parameters of surfaces by atomic force microscopy. *CIRP Ann.* **1995**, *44*, 517–522. [[CrossRef](#)]
8. Abe, H.; Nomura, T.; Kubota, Y. Lubrication of tube in cold pilgering. *J. Mater. Process. Technol.* **2014**, *214*, 1627–1637. [[CrossRef](#)]
9. Lin, H.S.; Marsault, N.; Wilson, W.R.D. A mixed lubrication model for cold strip rolling—Part I, Theoretical. *Tribol. Trans.* **1998**, *41*, 317–326. [[CrossRef](#)]
10. Montmitonnet, P.; Farrugia, D.; Aubin, J.L.; Delamare, F. Internal surface roughness of cold pilgered zircaloy pipes. *Wear* **1992**, *152*, 327–342. [[CrossRef](#)]
11. Yan, F.F. Pass Design of LG730 Cold-Rolling Pilger Mill and Its Finite Element Simulation in the Rolling-Process. Master's Thesis, Yanshan University, Qinhuangdao, China, 2015.
12. Li, H.; Wei, D.; Zhang, H.Q.; Yang, H.; Liu, H.R.; Liu, S.T.; Chu, Z.B.; Zhang, D. Texture evolution and controlling of high-strength titanium alloy pipe in cold pilgering for properties tailoring. *J. Mater. Process. Technol.* **2020**, *279*, 116520. [[CrossRef](#)]
13. Pocięcha, D.; Boryczko, B.; Osika, J.; Mroczkowski, M. Analysis of pipe deformation process in a new pilger cold rolling process. *Arch. Civ. Mech. Eng.* **2014**, *14*, 376–382. [[CrossRef](#)]
14. Li, X.; Zheng, J.; Yu, B.; Du, Y.; Zhou, Y. Analytical Model of Hole Diameter and Self-Guiding Machining Mechanism of BTA Deep Hole Drilling. *Materials* **2022**, *15*, 5329. [[CrossRef](#)] [[PubMed](#)]
15. Lili, L. Study on Radial Forging Process of Barrel and Properties of Forged Barrel. Ph.D. Thesis, Nanjing University of Science and Technology, Nanjing, China, 2013.
16. Tyagi, P.; Brent, D.; Saunders, T.; Goulet, T.; Riso, C.; Klein, K.; Moreno, F.G. Roughness reduction of additively manufactured steel by electropolishing. *Int. J. Adv. Manuf. Technol.* **2020**, *106*, 1337–1344. [[CrossRef](#)]